TWENTY FIRST EUROPEAN ROTORCRAFT FORUM

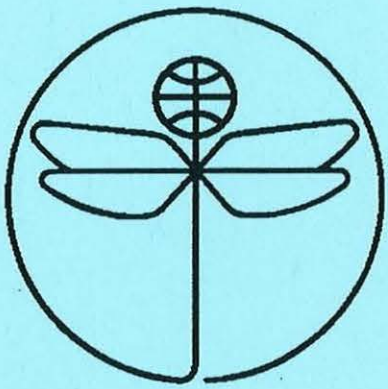

Paper No II.5

# HIGH RESOLUTION FREE VORTEX BLOB METHOD FOR HIGHLY DISTORTED VORTEX WAKE GENERATED FROM A SLOWLY STARTING ROTOR BLADE IN HOVER

**BY**

Duck Joo Lee, Seon Uk Na

DEPT. OF AEROSPACE ENGINEERING
Korea Advanced Institute of Science and Technology
KOREA

August 30 - September 1, 1995

SAINT - PETERSBURG, RUSSIA

Paper nr.: II.5

# High Resolution Free Vortex Blob Method for Highly Distorted Vortex Wake Generation from a Slowly Starting Blade in Hover.

**D.J. Lee; S.U. Na**

**TWENTY FIRST EUROPEAN ROTORCRAFT FORUM**
August 30 - September 1, 1995 Saint-Petersburg, Russia

# High Resolution Free Vortex Blob Method for Highly Distorted Vortex Wake Generated From a Slowly Starting Rotor Blade in Hover

Duck Joo Lee and Seon Uk Na
Dept. of Aerospace Engineering,
Korea Advanced Institute of Science and Technology, KOREA

## Abstract

The wake geometry of helicopter in hover is calculated by using a time accurate free vortex blob method without a non physical model of the far wake. The trailed and shed rotor wake are modeled by vortex blobs. This method has the advantage that the blobs are independent and free to move as they do not necessarily belong to a specific vortex filament for all times. This property is useful to investigate stable self vortex interaction and interaction. For the case of a rotor blade in hover, the lift and circulation distributions along the span are obtained, and the radial & axial geometries of the tip vortex are calculated. The numerical results are in good agreements with those obtained by the prescribed wake model of Kocurek and Tangler. The computed free wake geometry also agrees well with the wake geometry obtained from smoke visualizations.

## 1. Introduction

It is well known that the wake geometry of helicopter is critical in estimation of helicopter performance. So far, a prescribed wake model[1,2] or iterative free wake model[3-4] has been used by many researchers successfully to calculate the blade loadings in certain conditions. However, realistic geometry of the wake has not been predicted by using any other analytic or computational method.

Current methods of the wake analysis in helicopter flow field range from relatively simple momentum theory to free wake lifting surface methods. However, the inadequacy of these methods has led to recent efforts to use the computational fluid dynamics(CFD) codes,[5,6] which are widely used in fixed wing analysis. However, the state-of-the-art codes are insufficient for accurate predictions of general cases because they do not account for the rotor's extensive wake system. So, it is a recent trend to develop the wake capturing techniques that are able to predict the whole mechanism of the vortical flows, as computing power has progressively increased.

Whether iterative or time accurate free wake method, or CFD codes, the far wake model and the initial wake condition are essential to obtain a converged steady hovering solution. Typically, the far wake is modeled by a vortex ring[3] or a semi infinite cylinder[4] or the far wake is truncated after several spirals of the wake.[7]

The initial wake state is very critical especially for the time accurate method because of the instability of the wake. Therefore, a helicoidal spiral wake[7] is used initially or a uniform down velocity[9] is given to move the earlier vortex wake downward from the rotor disk to avoid problems due to the instability. However, the true transient solution and the wake mechanism can't be predicted.

The truly time marching free wake method has been tried to develop by authors[11], which doesn't need the non-physical initial condition and the near & far wake model. Therefore, the three regions of wake obtained from the smoke visualization as shown in Fig 1 can be predicted as well as the rotor blade loadings; well defined tip vortex region up to 3~4 revolutions, recirculation region due to vortex instability after 3~4 revolutions and expanded region of wake. Those objectives can be fulfilled not only by using the accurate numerical scheme, but also observing the physical phenomena carefully. One of the key point of our research is the increasing the rotation speed from zero to a required speed slowly to reduce initial vortex wake instability. The truly unsteady wake mechanism is very important to predict the unsteady loading & noise as well as the performance.

In this paper, the previous method developed by the authors is extended to account the sterength effect of the vortex filament by solving the vortex transport equation. The vortex segments are modeled as vortex blobs, which are free to move independently according to the Biot-Savart law and the vortex transport equation.

## 2. Formulation

The fluid surrounding the body is assumed to be inviscid, irrotational, and incompressible over the entire flow field, excluding the body's solid boundaries and its wakes. Therefore, a velocity potential $\Phi(x,y,z)$ can be defined and the continuity equation in the inertial frame becomes

$$\nabla^2\Phi = 0 \qquad (1)$$

The first boundary condition requiring zero normal velocity across the body's solid boundaries is

$$(\nabla\Phi - \vec{V}) \cdot \vec{n} = 0 \qquad (2)$$

Here, $\vec{V}$ is the body surface's velocity and $\vec{n}$ is the vector normal to this moving surface, as viewed from the inertial frame of reference. Since the governing equation does not depend directly on time, the time dependency is introduced through this boundary condition(the location and orientation of the vector normal to the moving surface can vary with time). For incompressible flows, the instantaneous solution is independent of time derivatives. That is, since the speed of sound is assumed to be infinite, the influence of the temporal boundary condition is immediately radiated across the whole fluid region. Therefore, the steady-state solution technique can be used to treat the time dependent problem by substituting the instantaneous boundary condition at each moment. The wake shape, however, does depend on the time

history of the motion and consequently an appropriate vortex wake model has to be developed.

The second boundary condition requiring that the flow disturbance, due to the body's motion through the fluid, should diminish at the far field from the body is as below;

$$\lim_{|R - R_\infty| \to \infty} \nabla\Phi = 0 \qquad (3)$$

For the unsteady flow field, the use of the Kelvin condition will supply an additional equation that can be used to determine the streamwise strength of the vorticity shed into the wake.

Using Green's identity, the general solution of (1) can be constructed by integrating the contribution of the basic solution of source($\sigma$) and doublet($\mu$) distributions over the body's surface and its wakes;

$$\Phi(X,Y,Z) = \frac{1}{4\pi}\int_{body+wake} \mu\vec{n}\cdot\nabla(\frac{1}{r})ds - \frac{1}{4\pi}\int_{body} \sigma(\frac{1}{r})ds \qquad (4)$$

The resulting velocity induced by the combination of the source($\sigma$) and doublet($\mu$) distributions is

$$\nabla\Phi = \frac{1}{4\pi}\int_{body+wake} \mu\nabla[\frac{\partial}{\partial n}(\frac{1}{r})]ds - \frac{1}{4\pi}\int_{body} \sigma\nabla(\frac{1}{r})ds \qquad (5)$$

Inserting equation(5) to equation(2) results

$$\{\frac{1}{4\pi}\int_{body+wake} \mu\nabla[\frac{\partial}{\partial n}(\frac{1}{r})]ds - \frac{1}{4\pi}\int_{body} \sigma\nabla(\frac{1}{r})ds - \vec{V}\}\cdot\vec{n} = 0 \qquad (6)$$

The source term is neglected in the case of small effect due to thickness of blade. Thus only the first part of (4) is used to represent lifting surface and wake element.

The constant strength doublet panel is equivalent to a closed vortex lattice with the same strength of circulation.($\Gamma = \mu$) The blade is represented by spanwise and chordwise distributions of vortex lattice.

Application of flow tangency condition(6) and representing the blade with the vortex lattice distribution yield the following linear matrix equation that is to be solved.

$$\begin{bmatrix} a_{11} & a_{12} & \cdots & a_{1n} \\ a_{21} & a_{22} & \cdots & a_{2n} \\ \vdots & \vdots & \ddots & \vdots \\ a_{n1} & a_{n2} & \cdots & a_{nn} \end{bmatrix} \begin{bmatrix} \Gamma_1 \\ \Gamma_2 \\ \vdots \\ \Gamma_n \end{bmatrix} = \begin{bmatrix} R_1 \\ R_2 \\ \vdots \\ R_n \end{bmatrix} \qquad (7)$$

Here $a_{ij}$ is the normal induced velocity coefficient on the i th element of blade due to the j th vortex lattice with unit circulation, and $\Gamma_j$ is the unknown circulation value of the blade vortex lattice. $R_j$ is the normal induced velocity at each control point due

to free stream velocity, blade moving velocity and wake induced velocity.

The aerodynamic loads of the blade can be calculated by using the unsteady Bernoulli's equation.

## 3.Time marching free vortex blob method

A three dimensional wing trails the bound circulation($\Gamma$) into a wake. Radial variation of $\Gamma$ produces trailed vorticity. Azimuthal variation of $\Gamma$ produces shed vorticity. The strength of the trailed and shed vorticity is determined by the radial and azimuthal derivatives of $\Gamma$ at the time the wake element leaves the blade. The bound circulation has a peak near the tip, and quickly drop to zero. The trailed sheet therefore has a high strength(proportional to the radial derivative of $\Gamma$) at the outer wake, and quickly rolls up into a concentrated tip vortex. The strength of shed wake vortex at this time step is set equal to the one of the vortex lattice, which is located at the trailing edge of the blade ($\Gamma_{T.E,t} = \Gamma_{wake,t}$). This condition is forced to satisfy the Kutta condition($\gamma_{T.E} = 0$).

The trailed and shed vortex element are modeled as vortex blobs in other words finite vortex sticks. A position vector and a strength vector are associated to each element. Each element can be thought of as a small section of a vortex tube. The element is convected by the local velocity and the strength vector is strained by the local velocity gradient. This method has the advantage that the blobs are independent to move as they do not necessarily belong to a specific vortex filament for all times. This property is useful to calculate self vortex interaction and interaction with other blades and fuselages.

The blob representing of the vorticity $\vec{\omega}_\sigma$ field is taken as

$$\vec{\omega}_\sigma(\vec{x},t) = \sum_p \vec{\omega}^p(t)\, vol^p\, \zeta_\sigma(\vec{x} - \vec{x}^p(t)) = \sum_p \vec{\alpha}^p(t)\, \zeta_\sigma(\vec{x} - \vec{x}^p(t)) \qquad (8)$$

where $\zeta_\sigma(\vec{x}) = \frac{1}{\sigma^3}\zeta(\frac{|\vec{x}|}{\sigma})$. is the regularization function which is usually taken as radially symmetric, and $\sigma$ is a smoothing radius. And $vol^p$ is the volume of the blob.

Then velocity field is obtained as

$$\vec{u}_\sigma(\vec{x},t) = \sum_p k_\sigma(x - x^p(t)) \times \vec{\alpha}^p(t), \qquad (9)$$

where $k_\sigma(\vec{x})$ is the regularized Biot-Savart Kernel.

The physical stretching phenomena of vorticity is also calculated numerically by solving the vorticity transport equation.

$$\frac{\partial\vec{\omega}}{\partial t} + (\vec{u}\cdot\nabla)\vec{\omega} = (\vec{\omega}\cdot\nabla)\vec{u} \qquad (10)$$

The evolution equations for the vortex blob position and strength vector are

taken as

$$\frac{d}{dt}\vec{x}^p(t) = \vec{u}_\sigma(\vec{x}^p(t), t) \tag{11}$$

$$\frac{d}{dt}\vec{\alpha}^p(t) = (\vec{\alpha}^p(t)\cdot\nabla^T)\vec{u}_\sigma(\vec{x}^p(t), t) \tag{12}$$

A 3D smoothing function is proposed by Winckelmans and Leonard[10] which is the high order algebraic smoothing: $\zeta(\rho) = \frac{15}{8\pi}\frac{1}{(\rho^2+1)^{7/2}}$. (13)

The equations obtained with this high order algebraic smoothing(13) is

$$\frac{d}{dt}\vec{x}^p = -\frac{1}{4\pi}\sum_q \frac{(|\vec{x}^p - \vec{x}^q|^2 + \frac{5}{2}\sigma^2)}{(|\vec{x}^p - \vec{x}^q|^2 + \sigma^2)^{5/2}}(\vec{x}^p - \vec{x}^q)\times\vec{\alpha}^p, \tag{14}$$

$$\frac{d}{dt}\vec{\alpha}^p = \frac{1}{4\pi}\sum_q \left[\frac{(|\vec{x}^p - \vec{x}^q|^2 + \frac{5}{2}\sigma^2)}{(|\vec{x}^p - \vec{x}^q|^2 + \sigma^2)^{5/2}}\vec{\alpha}^p\times\vec{\alpha}^q + \frac{(|\vec{x}^p - \vec{x}^q|^2 + \frac{7}{2}\sigma^2)}{(|\vec{x}^p - \vec{x}^q|^2 + \sigma^2)^{7/2}}(\vec{\alpha}^p\cdot((\vec{x}^p - \vec{x}^q)\times\vec{\alpha}^q)(\vec{x}^p - \vec{x}^q))\right] \tag{15}$$

Then the position and vorticity of the vortex blobs are simultaneously updated at each time step using the Biot-Savart law(14) and the vorticity equation(15).

## 4.Results and Discussions

The wake geometry and the blade loading of a single blade rotor with rectangular planform are calculated, and compared with the results of prescribed wake and experimental results. The rotor blade is modeled using 5 chordwise panels and 15 spanwise panels. The aspect ratio of the blade is 6.54. The chord length is taken as 1.0. Time step per one revolution is taken as 24. And the angular velocity of the rotor is 503 rpm.

*Instability of impulsively starting vortex*

It is notorious that the wake becomes unstable after a few spirals of the wake.(Fig 3) The strong instability of the initial wake can be overcome by observing the real phenomena of the rotating blade. That is, the rotor rotates from zero to a certain steady r.p.m. smoothly. This approach is critical which is validated by using the curved vortex filament for the simulation of hovering rotor wake.[11] Then the strength of the initial wake is weak, the instability of wake is suppressed, and the wake moves downward slowly.

*Instability of recirculated wake*

The starting wake rolls up into a concentrated tip vortex in the outer part of the blade. The tip vortex, clearly shown in the smoke visualization(Fig 1), moves

downwards during 3~4 revolutions to be unstable again. Then, the tip vortex stays in a certain distance from the rotor disk and does not move downward anymore. Several spirals of the vortex interact strongly at the position to become a strong vortex bundle, called as a recirculated region of the wake.

No clear smoke visualization can be seen in the region except several tip vortex locations due to smoke diffusion and viscous diffusion. Most numerical results enforcing the initial and the far wake conditions show many revolutions of the clear tip vortex without instability, which are different from the real wake.

The recirculated unstable wake after the clear tip vortex revolution is obtained by using present time marching wake as shown in Fig 4, Fig 5 and the cross sections of the roll up and expanded wake geometry is shown in Fig 6. Not only the tip vortex but also the vortex sheet shed from the inner part of the blade becomes unstable. After the maximum contraction, the wake expands rapidly. The 10 revolutions are necessary to obtain the steady state of wake geometry up to one revolutions from the rotor blade as shown in Fig 7, and the 12 revolutions are necessary up to three revolution from the rotor blade.

*Comparison of the wake geometry and loadings*

The calculated values of the radial location of the tip vortex are compared with the prescribed wake geometry as shown in Fig 8. The figure shows that the contraction of the tip vortex increases as the wake azimuth angle increases. The calculated value of the axial location of the tip vortex is also shown in Fig 8. The tip vortex descent rate is constant up to 360 degrees for the single blade rotor. After this azimuth angle, the descent rate increases. The calculated spanwise lift and circulation distributions by using the present free wake method are also compared with the prescribed wake results as shown in Fig 9, and Fig 10.

## 5. Concluding Remarks

Wake geometries and blade loadings of helicopter in hover are calculated by using a truly time marching free vortex blob method without a non physical model of the far wake. The vortex blob method has the advantage that the blobs are independent to move as they do not necessarily belong to a specific vortex filament for all times. This property is useful to stabilized the self vortex interaction and interaction with other blades and fuselages. And the truly unsteady wake mechanism is very important to predict the unsteady loading & noise as well as the performance.

The strong instability of the initial wake can be overcome by slowly rotationg the blade. Then the strength of the initial wake is weak, the instability of wake is suppressed, and the wake moves downward slowly.

For the case of rotor blade in hover, the thrust and the circulation distribution along the span are obtained and the radial & axial geometries of the tip vortex are calculated without a far wake model. The numerical results are in good agreements

with the results obtained from the prescribed wake model of Kocurek and Tangler[2].

The computed free wake geometry is also at least qualitatively in good agreement with the experimental wake mechanism which is represented by three wake regions. The result indicates that the classical wake concept is wrong which is represented by the smoothly contracted tip vortex trajectory extended to the far down stream.

It is also expected that the unsteady loadings occuring in forward flight or coaxial helicopter can be predicted by the present time marching free vortex blob method.

## References


1. Landgrebe, A. J. The Wake Geometry of a Hovering Helicopter Rotor and Its Influence on Rotor Performance. Journal of the American Helicopter Society, Vol. 17, Oct. 1972, pp. 3-15.
2. Kocurek, J. D. and Tangler, J. L. A Prescribed Wake Lifting Surface Hover Performance analysis. Journal of the American Helicoper Society, Vol. 22, (1),Jan.1977, pp. 24-35.
3. Clark, D. R. and Leiper, A. C. The Free Wake Analysis a Method for The Prediction of Helicoper Roter Hovering Performance. Journal of the American Helicoper Society, Vol. 15, (1), Jan. 1970, pp. 3-11.
4. Rosen, A. and Grabe, A. Free Wake Model of Hovering Rotors Having Straight or Curved Blades. Journal of the American helicoper Society, Vol. 33, (3), July ,1988, pp. 11-19
5. G.R.Srinivasan, J.D. Baeder, S. Obayashi, and W. J. McCroskey. Flowfield of a Lifting Rotor in Hover: A Navier-Stokes Simulation. AIAA Journal, Vol. 30, No. 10, Oct. 1992, pp. 2371-2378.
6. Strawn, R. C. and Barth, T. J. A Finite-Volume Euler Solver for Computing Rotary-Wing Aerodynamics on Unstrained Meshes. Journal of the American Helicopter Society, Vol. 38, April 1993, pp. 61-67.
7. Morino, L., Kaprielian, Z. and Sipcic, S. R. Free Wake Analysis of Helicopter Rotors. Ninth European Rotorcraft Forum, Stresa, Italy, Sept.1983,Paper No. 3.
8. Wayne Johnson. Vortex-Induced Velocity. Helicopter Theory, Princeton University Press, 1980, pp. 535-547.
9. Katz, J. and Maskew, B. Unsteady Low-Speed Aerodynamic model for Complete Aircraft Configurations. Journal of Aircraft, Vol. 25, No. 4, 1987, pp. 302-310.
10. S. Winckelmans and A. Leonard. Contributions to Vortex Particle Methods for the Computation of Three-Dimensional Incompressible Unsteady Flows. Journal of Computational Physics, Vol. 109, 1993, pp 247-273
11. D. J. Lee and S. U. Na, Predictions of Helicopter Wake Geometry and Air Loadings by using a Time Marching Free Wake Method. The 1st Forum Russian Helicopter Society, 1994

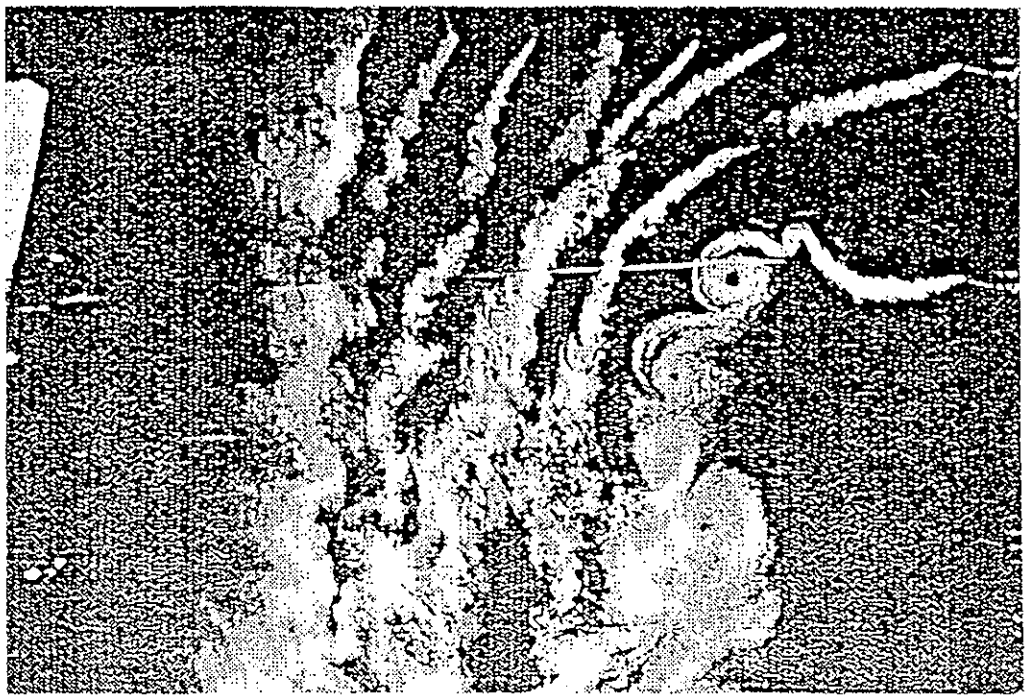

Fig 1. Rotor wake flow visualization[1]

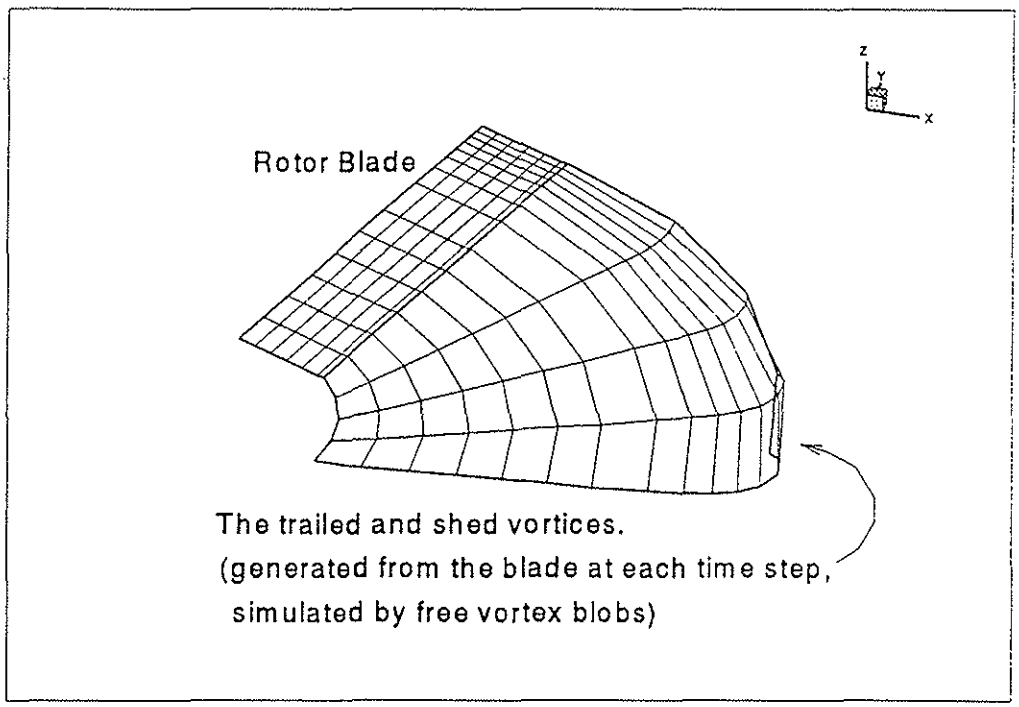


Fig 2. The schematic view of the hovering rotor wake

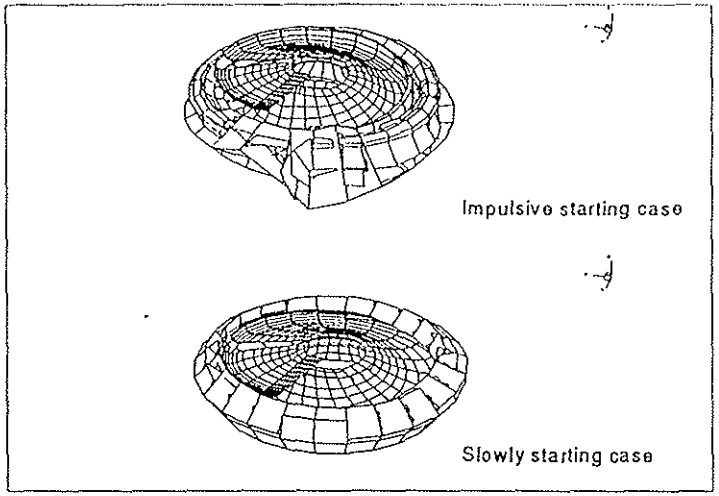


Fig 3. The calculated free wake geometry for the impulsive starting rotor and slowly starting rotor (at 4 revolutions)

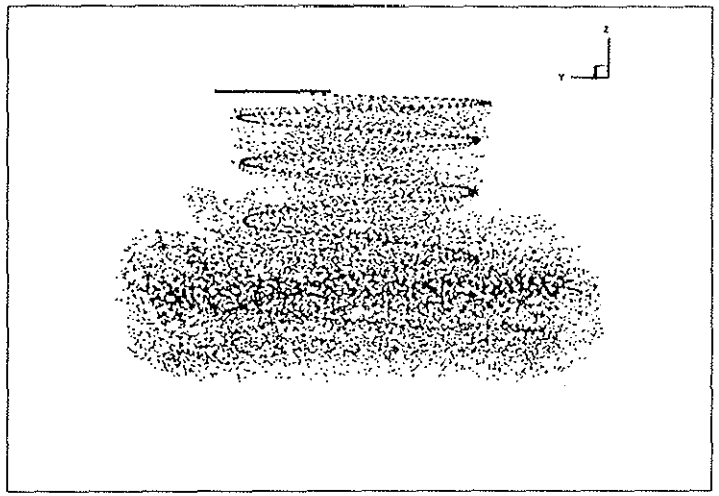

Fig 4. The side view of a calculated free wake geometry



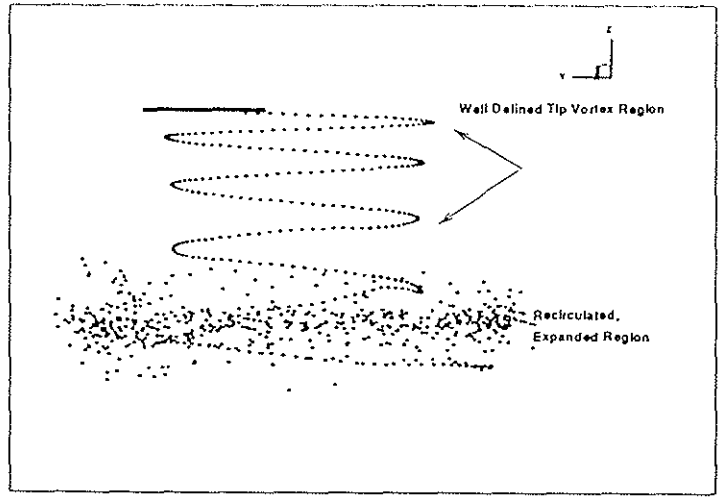


Fig 5.The side view of a calculated free wake tip vortex geometry

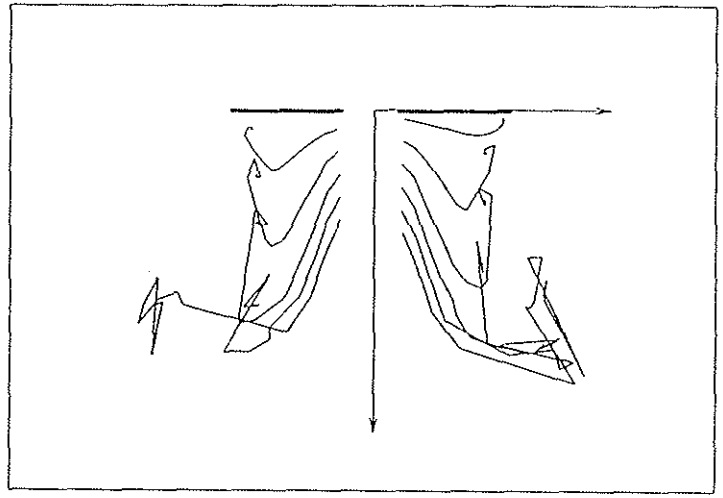

Fig 6.The cross sections of the wake at various azimuth angle

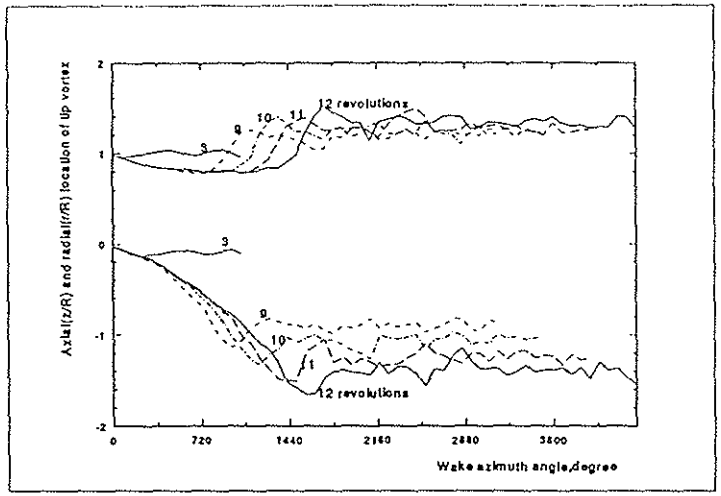


Fig 7. The time history of the tip vortex axial and radial locations

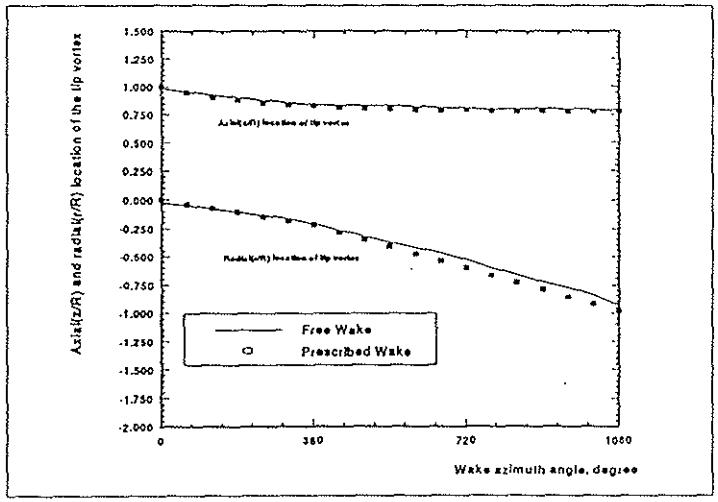


Fig 8. Comparison of the tip vortex axial and radial locations between the free wake and prescribed wake results



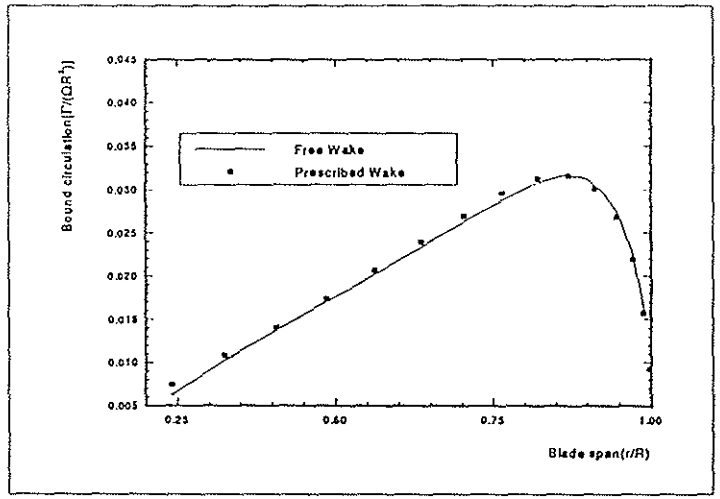


Fig 9. Comparison of the spanwise thrust distributions between the free wake and prescribed wake results.

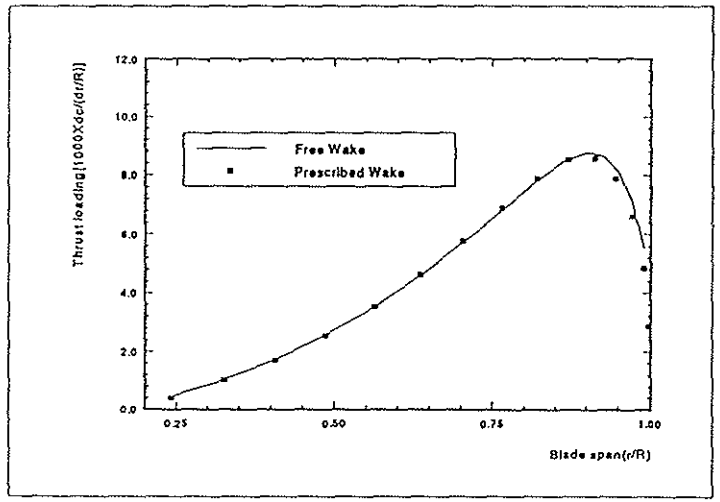


Fig 10. Comparison of the spanwise circulation distributions between the free wake and prescribed wake results.